Heliyon 10 (2024) e29986

Contents lists available at ScienceDirect

Heliyon

journal homepage: www.cell.com/heliyon

Research article

A novel in-situ dynamic mechanical analysis for human plantar soft tissue: The device design, definition of characteristics, test protocol, and preliminary results

Longyan Wu [a,1], Ran Huang [a,b,c,*,1], Lisheng Tang [c,1], Xinyi Ning [a], Jun Zhu [b,**], Xin Ma [a,d,***]

[a] Academy for Engineering and Technology, Fudan University, Shanghai, 200433, China
[b] Yiwu Research Institute of Fudan University, Yiwu, Zhejiang, 322000, China
[c] Center for Innovation and Entrepreneurship, Taizhou Institute of Zhejiang University, Taizhou, Zhejiang, 318000, China
[d] Shanghai Sixth People's Hospital, Shanghai Jiao Tong University, Shanghai, 200233, China

ARTICLE INFO

Keywords:
Plantar soft tissue
In-vivo
In-situ
Dynamic mechanical analysis
Biomechanical characterization

ABSTRACT

The in-situ mechanical characterization of elastomers is not highly regarded due to the existence of a well-established set of sample-based standard tests for research and industry. However, there are certain situations or materials, like biological soft tissue, where an in-situ approach is necessary due to the impossibility of sampling from a living body. We have developed a dynamic mechanical analysis (DMA)-like device to approach *in-vivo* and in-situ multidimensional stress-strain properties of human plantar soft tissues. This work elucidates the operational mechanism of the novel measurement, with the definition of a new set of moduli, test standardization and protocol. Exploratory results of a volunteer's living plantar, silica rubber samples are presented with well preciseness and consistence as expected.

1. Introduction

The plantar soft tissue, located between the dermis and bones of foot, is a critical composite material integrated of fat and specific connective tissue [1] to cushion shock, absorb impact [2,3], and protect against excessive local stress [4] for our daily locomotion and weight-bearing activities. Given the feature of shape recovery and energy dispersion, biological soft tissue is generally taken as elastomer in the field of biomaterials and biomechanics; and artificially synthesized elastomers of moduli in the MPa range can be easily tuned to match well with the mechanical properties of soft tissues [5]. Thereafter, the characterization of mechanical properties of soft tissue is a key content in the field of clinical medicine, biomedical engineering, and bionic materials [6,7].

The stress-strain mechanical test methods for industrial elastomer are therefore applied onto biological soft tissues [8], usually with cadaveric specimens [9], whereas live specimens are strictly impossible, and even experiments targeting animal organs are difficult to achieve and require very strict conditions and ethical permission. However, the obvious difference between ex-vivo specimen and

* Corresponding author. Academy for Engineering and Applied Technology, Fudan University, Shanghai, 200433, China.
** Corresponding author.
*** Corresponding author. Academy for Engineering and Applied Technology, Fudan University, Shanghai, 200433, China.
E-mail addresses: huangran@fudan.edu.cn (R. Huang), zhujun@ywfudan.cn (J. Zhu), xinma_faet@fudan.edu.cn (X. Ma).
[1] L.W., R.H. and L.T. contributed equally to this work.

https://doi.org/10.1016/j.heliyon.2024.e29986
Received 11 December 2023; Received in revised form 17 April 2024; Accepted 18 April 2024
Available online 20 April 2024

living tissue in the biochemical state and mechanical properties makes it controversial and lack of feasible cross check.

Current material characterizations of living tissues are mainly carried by ultrasound and imaging due to their non-invasive feature [10–12]. However, imaging methods are subject to exposure and have strict limitations on the number of measurements and irradiation time. Moreover, these indirect methods can only provide discrete stress-strain data, which makes the construction of constitutive equation difficult.

Over the past decades, dynamic mechanical analysis (DMA) has become a standard tool for materials research to approach the periodic strain-stress behavior, elasticity, and viscosity [13,14]. A number of DMA tests were reported on ex-vivo cadaveric specimens, whereas the defects are obvious [15]. In recent years, some researches have adopted *in-vivo* indentation tests via a single pulse to access the force-displacement and stress-relaxation curves [16], and achieve half of the periodic dynamic stress-strain correspondence. Yet continuous and full-periodic mechanical measurements on living tissues, as an ideal methodology, has not been reported in the field.

In-situ and *In-vivo* mechanical tests on plantar soft tissue, if being made feasible, are not only of importance in precise measurement comparing to the cadaveric tests, but also implies significant potentials in clinics and healthcare. The variations in the soft tissue's mechanical characteristics at different plantar locations may indicate health or even pathological issues. For instance, the soft tissue stiffening under the metatarsal heads may lead to foot ulcers in diabetics [17] and metatarsalgia in the elderly [18]; It has also been demonstrated that altered mechanical properties of the heel pad may result in shock-induced injuries such as heel pain and Achilles

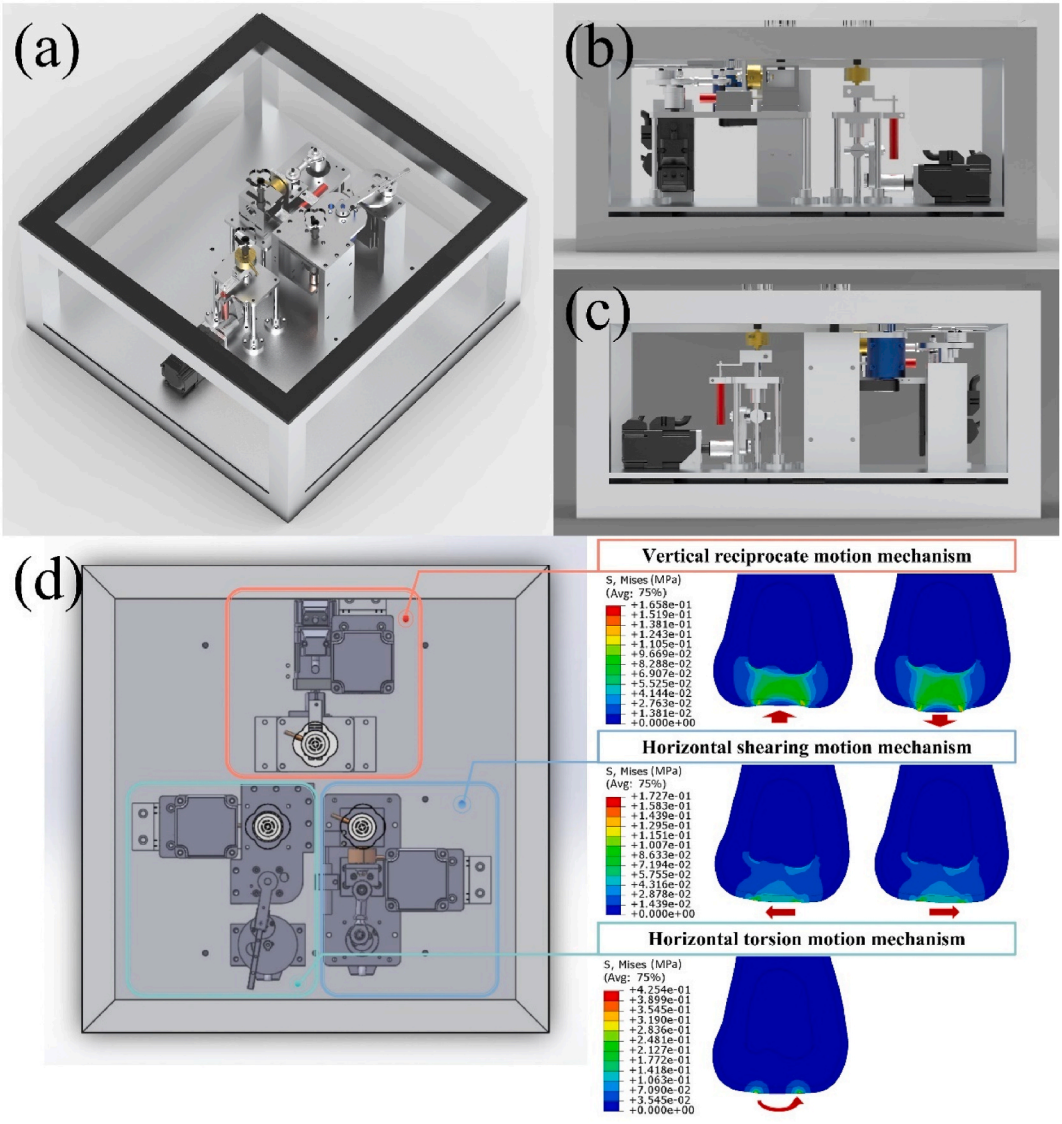

Fig. 1. Mechanical drawing of the in-situ DMA device to measure the material properties of plantar soft tissue: (a) The axonometric view; (b) The left-side view; (c) The right-side view; (d) The upper view and the demonstration of three functional units for measurements in three directions: tensile/compression, horizontal shear and torsion.

tendinitis [19]; Since soft tissue properties vary remarkably across different plantar regions [20], the real-time monitoring on the material properties on the living plantar are necessary as a clinical examine [21], whereas ex-vivo test has no way to be useful in this mean.

During daily activities, the planter soft tissue bears mechanical loads and land forces in various dimensions: i.e., pressure acting normal to the land and shear stress acting tangential to the plantar surface [22]. For various orthopedic or systemic diseases, it can be of great interest to learn the effects of different forms of stress onto the human foot. While so far vertical pressure has been widely reported, there are very few studies on shear and torque [23]. One probable reason may be the lack of available device and methodology for the shear and torque measurements, especially *in-vivo* and in-situ [24].

In response to the above concerns, we have invented a device based on the principle of DMA to measure the *in-vivo* and in-situ material properties of soft tissue, especially for plantar. The engineering verification of the design has been done in simulation, and consistent theoretical results has been achieved to certify its capability to measure the periodic strain-stress behavior, and analyze the material properties in a continuous fashion [25–27]. With the periodic strain-stress measurement, the mathematic processing of constitutional equation of viscoelasticity via phase lag analysis is made possible, which is the classical methodology for conventional elastomeric materials. In this manuscript, the mechanical design and working principle of the in-situ DMA-like device is described in details (section II), the characteristics, i.e., a set of moduli, for soft tissue in this newly-invented test are defined (section III), the sample standardization and calibration is carried out with the help of finite element analysis (FEA), as a common tool in biomechanics [28,29] (section IV), the test protocol on living plantar is settled (section V), and finally, the preliminary results of testing on a living planter, a silica rubber mimic foot, and a silica rubber brick sample have been delivered as examples (section VI).

2. Device design

2.1. Mechanical structure

The application of periodical stress-strain onto plantar and the corresponding monitoring mainly involves sinusoidal motion of detector and its effective adhesion onto the subject, with precise add-on of force and distance sensor. Axonometric views (Fig. 1a), left- and right-side views (Fig. 1b and c), and the upper view of the device were displayed in Fig. 1, along with three stress-strain detecting units (Fig. 1d) that were arranged in a supporting framework and had a cover lid with three holes on it that allowed the plantar test-points to be subjected to the detector head. Moreover, a vacuum suction cup is set onto the head to firmly bound the plantar, and enables the reciprocal motion of soft tissue. The mechanical structure design of the three detection units can be simplified as sine mechanism, as shown in Figs. 2–4.

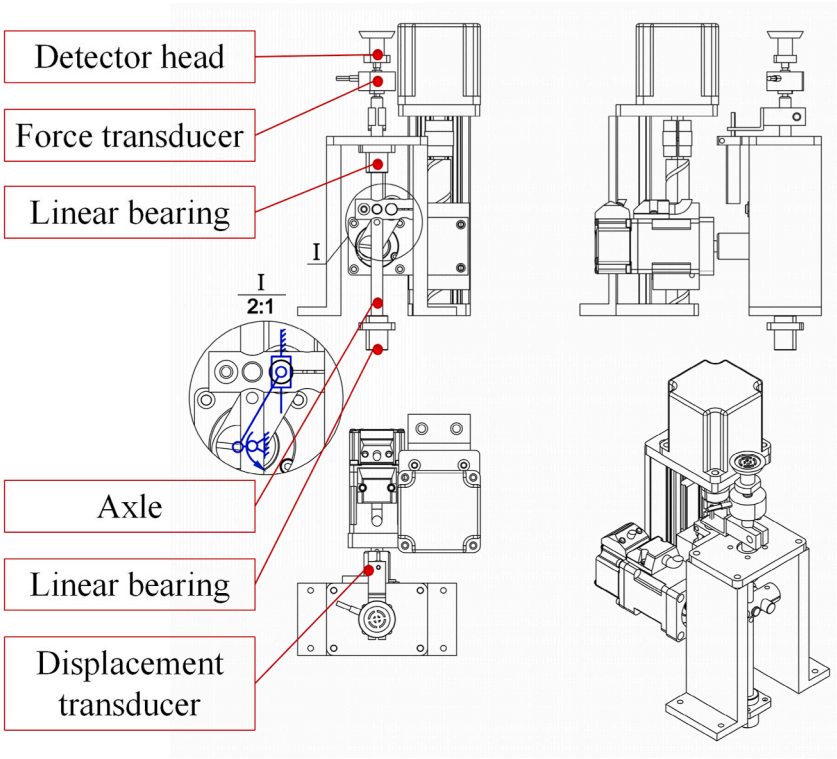

Fig. 2. The kinematic sketch of the mechanical structure of the vertical reciprocal motion mechanism.

The mechanical design of vertical reciprocal motion can be simplified as the crank slider mechanism, as shown in Fig. 2. By rotating the disk, along with the eccentrically mounted tie rods, the shaft makes reciprocating linear motion vertically under the limitation of the linear bearing. The force sensor and probe head are mounted sequentially on the shaft, while the displacement sensor is mounted on a fixed plate. One thing shall be addressed here, although the displacement is determined by the mechanical structure, e.g., the size of rotary disk, the eccentrical radius and the length of rod and so on, depending on the stiffness of subject, and inevitable errors, the actual strain happens on the subject may not be the set of displacement, which are observed many times in our following practice, therefore an independent displacement sensor is necessary. And this difference will be discussed in the results section. The mechanism of shearing motion can also be simplified as the crank slider, only that in a horizontal way, as shown in Fig. 3.

The horizontal torsion motion can be realized by crank rocker mechanism, as shown in Fig. 4. With the rotary of disk, the slider mounted eccentrically on the disk through the bearings rotates and drives the lead rail to swing cyclically. The torque sensor connected to the torsion axle monitors the oscillation via a synchronous belt. And torsional deformation is recorded by the angle transducer.

Moreover, each unit is equipped with a set of lifting mechanisms, allowing the detector to automatically rise during testing. After touching the plantar, the appropriate height is determined based on a default stress threshold, and the mechanism is fixed at that initial position. Then vacuum is applied to adhere the soft tissue. This is to avoid subjective force errors caused by subject actively adjusting the height of the foot to match the probe. As shown in Fig. 5, the mechanical principle is a nut-screw rotation, with a self-locking brake motor to keep the zero-position unchanged during the reciprocating test.

To ensure non-destructive and non-invasive binding, a vacuum composite suction cup is designed for the detector joint during the inspection (Fig. 6). The suction cup is composed of a rigid inner core and an elastic skirt edge. The upper surface of cup is designed with support ribs to ensure a stable and flat contact onto the tissue, and avoid shape change of the testing tissue. Also, this design can increase adherence intensity by lower the contact area with the same vacuum degree. Our practice verified that this design can firmly adhere the soft tissue under particular testing condition. The vacuum is provided by a regular laboratory oil pump with degree to be sufficient for the suction without the uncomfortable feeling reported by subjects.

2.2. Sensor models

We employed mature commercial sensors for force [30], torque [31], displacement [32] and angle [33] detection in the device. The vertical reciprocate mechanism is equipped with the force sensor (DYMH-103, Bengbu Dayang Sensing System Engineering Co., Ltd) and LVDT (Linear Variable Differential Transformer, GA09, Shanghai Utmost Electronics Co., Ltd). The sensor for the shearing mechanism is the same as that for the vertical, only that in a horizontal way. In the horizontal torsion mechanism, the torsional deformation and torque are recorded by torque sensor (FYAH, Forsentek Co., Ltd) and angle sensor (GT-D, Taizhou Quantum Electronic Technology Co., Ltd.). The specifics of sensors are listed In Table 1, and these have been proved to be well satisfactory for our test requirements. The data-acquisition (DAQ) consists of a USB 3151 unit (Art Beijing Science and Technology Development Corp., Ltd) configured for taking analog measurements with a 16-bit A/D converter at a sampling rate (Fs) of 500 kHz, satisfying the Nyquist

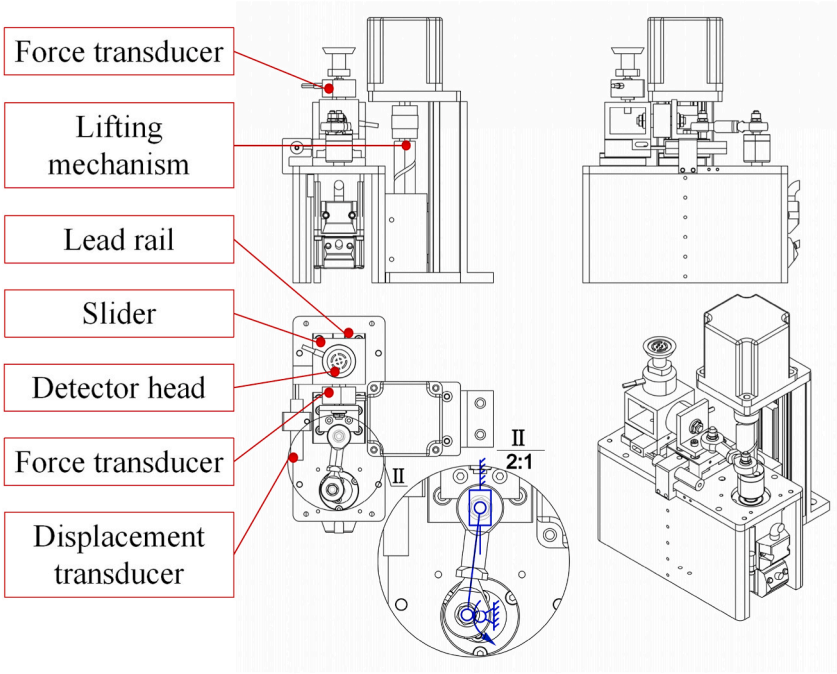

Fig. 3. The kinematic sketch of the mechanical structure of the horizontal shearing reciprocal motion mechanism.

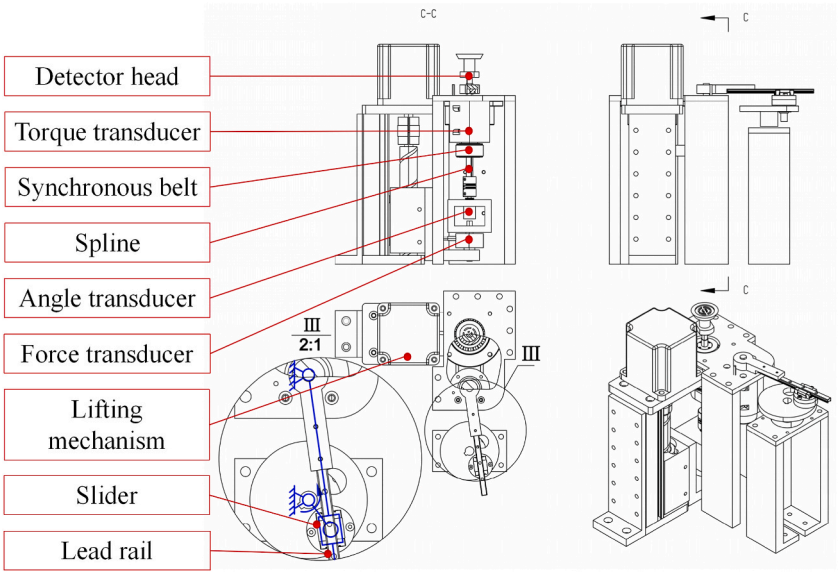

Fig. 4. The kinematic sketch of the mechanical structure of the horizontal torsion reciprocal motion mechanism.

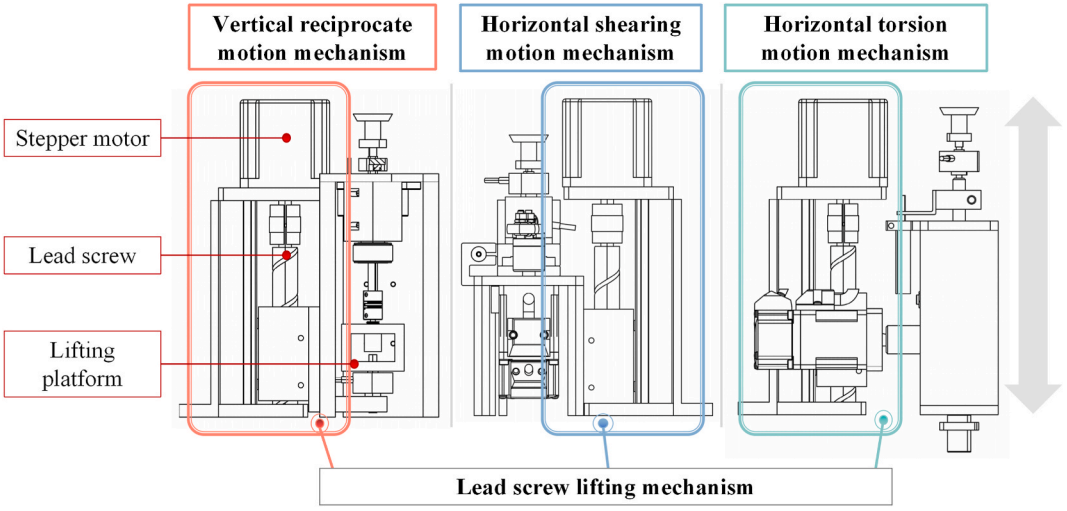

Fig. 5. The design of lead screw lifting mechanism.

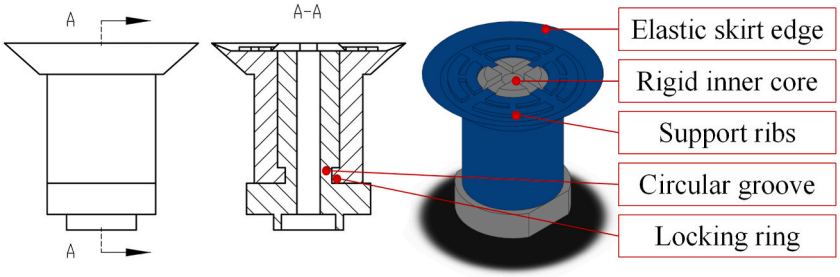

Fig. 6. The design of the mechanical structure of vacuum suction cup.

Table 1
Specifics of the sensors.

Sensor	Specifications	Values
Force sensor (DYMH-103)	Capacity	0–5 kg
	Response frequency	10 KHz
	Output sensitivity	1.0–1.5 ± 10 % mV/V
	Hysteresis	0.1 % F.S.
	Repeatability	0.1 % F.S.
	Temperature sensitivity drift	0.1 % F.S./10 °C
	Zero temperature drift	0.1 % F.S./10 °C
LVDT (GA09)	Capacity	±5 mm
	Response frequency	1-10 KHz
	Nonlinearity error	±0.5 % BFSL
Torque sensor (FYAH)	Capacity	0–1 NM
	Response frequency	200 Hz
	Nonlinearity	±0.25 % of R.O.
	Hysteresis	±0.25 % of R.O.
	Nonrepeatability	±0.1 % of R.O.
Angle sensor (GT-D)	Capacity	0–360°
	Resolution	4096, 12 bits
	independent linearity	0.15 % F.S.
	Response frequency	5 KHz
Module	Specifications	Values
DC signal isolator (0–10 V)	Standard accuracy	Typical value ± 0.1 % FS
	Temperature drift	Max. ± 0.005 %/10 °C
	Response time	<10 ms

criterion [34]. A DC signal isolator (Hangzhou Hengyi Instrument Technology Co., Ltd) is used to output DC signals to control systems or other instruments after processing such as isolation and interference suppression for more efficient signal processing. The specifics of the isolator are also listed in Table 1. Furthermore, FFT and cross-correlation analyses were performed on the load (stimulus) and deformation (response) signals. The spectrogram shows that the peak frequencies of the two signals are identical. The cross-correlation analysis identified a maximum cross-correlation of 0.9559 between two signals, along with a lag of 0.003s, indicating a strong correlation and minimal impact from lags on the results.

3. Definition of characteristics

In classical material mechanics, moduli are conducted by the relative change of stress (force) and strain (size change), e.g., the Young's modulus of tensile/compression is defined as $E = \sigma/\varepsilon = (\Delta F/A)/(\Delta L/L)$, where involves the original shape (L). However, while the strain here is a rigorous definition with exact shape and measures of the test sample, and the determination of these parameters is trivial in common material test, the subject we are dealing with in the new in-situ test has mere measures on shape and size (even if we can do exact measurements in some cases), either for biological tissue or inorganic object. Because the test is applied on a small area of the outer surface of a relatively large sample, the strain is obviously not only the shape change of the cylinder behind the suction area, therefore the original size L of this cylinder is regardless of the "modulus" interested in the present case, as the area marked out by the orange rectangle in Fig. 7. Fig. 7a is the FEA simulation of the in-situ tensile on a silica rubber brick sample. Although we have determined the effective strain depth is ~5 cm in this case of brick sample [27], it is still mysterious to approach the shape and size of an "equivalent cylinder". And for biological tissue, the dilemma is more complicated, the original shape and size of soft tissue is extremely difficult to be measured, and it almost differs in every individual case. Although we can somehow measure the thickness of

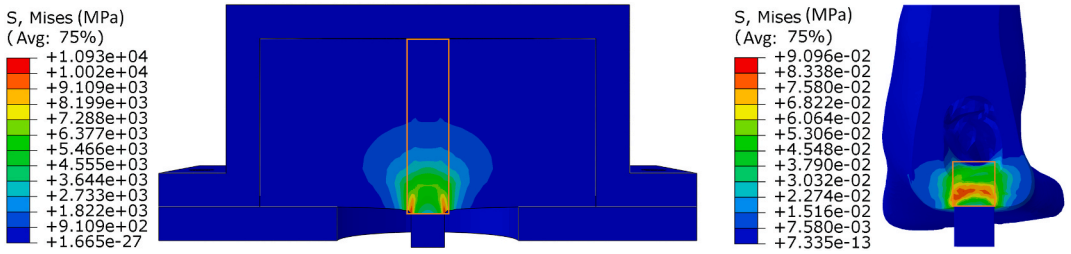

Fig. 7. FEA demonstration of the in-situ tensile on (a) silica rubber brick sample and (b) plantar heel model with skin (rear sectional view). The cylinder portion behind the suction area is marked out by the orange rectangular. It is clear the stress-strain behavior here is loosened out of the shape and size change of the cylinder, where a much more complicated strain map is involved, and the situation is more complicated in living plantar tissue of irregular shape and skin confinement. (For interpretation of the references to color in this figure legend, the reader is referred to the Web version of this article.)

plantar tissue, i.e., the distance from skin to the lower end of calcaneus, as the area marked in Fig. 7b, when the detector drives the motion of the suction area, it is easy to image that the whole plantar tissue around (without clear boundary) involves in the shapes change, and even worse the confinement of skin plays crucial role in the stress response, it is meaningless to define the original L here.

On the other hand, it is not unreasonable to doubt if this parameter is necessary in biomechanical characterization. Since we have exactly measurable force (or stress with area) and displacement (strain), given the L temporarily undefined, we may firstly define a series of "apparent moduli" analog to classical moduli: Similar to the classical Young's modulus, we define the tensile/compression combined modulus as

$$H_{TC} = \frac{F_{TC}/A}{\Delta L/L} \tag{1}$$

where F_{TC} is the force of both push and pull, A is the area of suction, L is the "original" length, and note the ΔL is the displacement of up and down.

Then the new shear modulus is defined as

$$H_S = \frac{F_S/A}{\Delta x/L} \tag{2}$$

where F_S is the force of shearing of two directions, and note the Δx is the displacement of tissue sheared to both sides. Due to the relationship between shear and torsion, we have the applied torque T (in the unit of $N{\cdot}m$) as

$$T = \frac{J_T}{L} H_S \varphi \tag{3}$$

where φ is the angle of twist in radians, and J_T is the torsion constant in the unit of m^4, although it firmly depends on the shape of object, and is complicated to determine for irregular shapes, fortunately we can simply derive it, without knowing the exact form in the means of geometry, from Eqns. (2) and (3):

$$J_T = \frac{TA\Delta x}{F_S \varphi} \tag{4}$$

Then we have the analog torsion modulus (or torsional rigidity analog to classical definition) in the unit of $N{\cdot}m^2$

$$H_T = J_T H_S = \frac{TA\Delta x}{F_S \varphi} H_S \tag{5}$$

Note that in the real test of plantar, there are two modes of shearing test (longitudinal and transverse), and correspondingly two moduli H_{LS} and H_{TS}, the H_S in Eqn. (5) is taken as $(H_{LS} + H_{TS})/2$ in practice.

Here the only undetermined variable is L, but whatever it may be, it does not affect the parallel comparison between the moduli in the same category among the tests. The definition can certainly fulfil our current needs to measure and examine the plantar tissue as a healthy indicator, by considering the shape and size are also part of the "eigen" tissue properties to be reflected by the stress-strain behavior, the term "apparent moduli" objectively characterize the properties of a particular tissue. In this way, we may set a nominal value of L to balance the dimension of equations. Currently this parameter is set to be 10 mm.

In the future research, with a large number of testing data, we expect to employ machine learning to figure out the underlying correlations and establish a reliable relationship between newly-defined analog moduli H and classical moduli G with a so-called "equivalent length" L. (This work is currently in progress in our group, since it is not a main concern in this work, we hope the results will be reported in near future).

4. Standard sample and calibration

The main idea of the in-situ test is a compromise for the strong limit of living tissues, as the test conditions such as force, frequency, temperature and so on are strictly confined within a tiny window. However, as a characterization itself, the determination of test limits requires samples beyond the coverage. Note that, the force and torque sensors employed in the instrument are mature industrial products and their calibration is trivial. The general procedure here is to correct the operational or systematic error.

On the other hand, a series of standard samples for calibration and correction is a must for a standardized characterization, while obviously the living tissue cannot serve this role, in either concern of standard materials or availability. In this work, the silicon rubber (SR) is selected to approximate the heel pad tissue. With present knowledge of the living tissue, the grade of SR is chosen as the tensile modulus of 0.518 MPa, compressive modulus of 1.228 MPa, elongation at break of 363.4 %, hardness of 18 (shore A), and density of 1.086 g/cm^3.

We employ a SR brick measuring $10 \times 10 \times 5$ cm^3 to test as a reference because the shape of a mimic foot cannot be a standard form of samples and lacks systematical comparability. A metal box covers the brick to act as the frame holder and give a rigorous confinement. In our earlier work [27], with the help of FEA, an ignorable boundary condition was sought to determine the shape and size of the brick sample in order to guarantee that the size is large enough to reflect the eigne properties of the elastomer regardless of the impact of size or boundary morphology. For the silica rubber employed in this case, that boundary was determined to be $5 \times 5 \times 2.5$ cm^3, thereby the current size is doubled to ensure the sufficiency.

It should be noted that here the size and material property of "standard" brick sample are merely artificial choice. Since our research focused on the biological soft tissue, especially the plantar, we select this grade of silica rubber for a standard sample. Nevertheless, this in-situ DMA method can also be expected to apply to the research of other soft matters, and depends on the objects it is meant to measure, the standard sample for calibration is a free choice. The basic principle is a reproducible elastomer to calibrate the machine, with sufficient size and regular shape to avoid the geometrical effect, and there is no necessity to rule a universal "standard" sample.

5. Test protocol

5.1. Test protocol for the volunteer participant

A volunteer participant (female, age: 30–35 yr, height: 165–170 cm, weight: 65–70 kg, body mass index (BMI): 23–25) (the personal info is reported in interval to protect privacy) has taken the test and been reported in this manuscript. The subject was required to have had no trauma to its feet in the past 12 months before data collection, and the plantar shall be observed to be in a healthy state, that appears not to have any injuries, infections, or pain. The assessment is done by researchers who have been trained by professional clinician in our group. Prior to testing, we explained the procedure and purpose of our study to the subject, collected personal and clinical information such as age, height, weight, foot length, foot width, footwear preferences, est. average steps per day, and exercise habits from the subject, which was subsequently anonymized during the data processing phase. The subject voluntarily signed the testing protocol agreement before testing commenced. The Ethical Review Committee of Huashan Hospital, Fudan University (HIRB) approves the ethical review (see the supplemental materials).

Due to the significant heterogeneity of plantar, the shearing along different direction is quite considerable, which also accords to the functionality of plantar. Thus, as mentioned above, in practice we take two modes of shearing test in longitudinal and transverse directions, that is, the direction from heel to toe, and vertical to the foot. In this way, the tests in four directions were carried out respectively at five spots on plantar tissue that are considered to be critical in bear-loading or prone to ulceration, including the three spots on the forefoot (the first, second, and fifth metatarsal heads), the midpoint on the lateral edge of the arch, and the center of the heel [21], as shown in Fig. 8.

The positions of test sites are determined with a series of references, where researchers have common concerns that specific points are crucial for plantar functioning. Referring to previous studies on foot morphology [35] and plantar pressure [36], the test on heel,

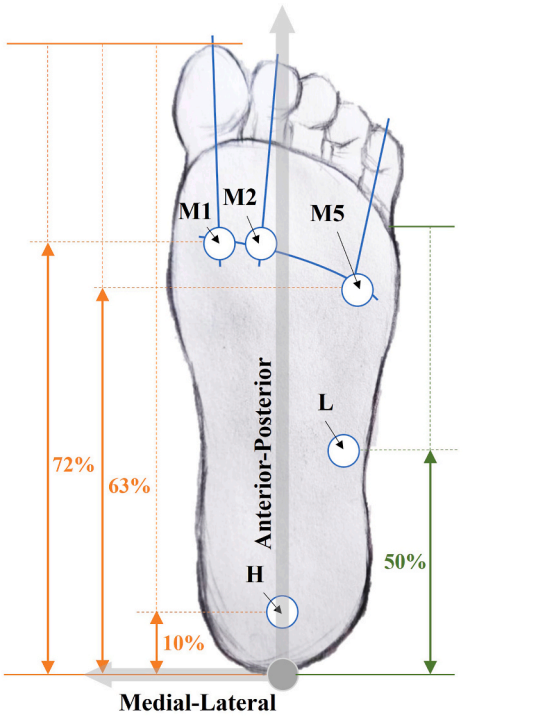

Fig. 8. Test locations of plantar soft tissue at the first, second, and fifth metatarsal heads (M1, M2, and M5), midpoint of lateral edge (L), and Heel (H). Note that the 50 % on the right to determine L is colored differently because it is based on a different 100 % norm.

the fifth, and the first metatarsal heads are positioned at around 10 %, 63 %, and 72 % of the foot length measured from the posterior-most point in the anterior–posterior direction. According to the distribution of pressure on the plantar [37–39], the line M1-M2 is considered perpendicular to the longitudinal direction, and these two are located at the cross-point of the 72 % "meridian" and the axis of first and second metatarsal bone, respectively. Similarly, M5 is located at the cross-point of the 63 % "meridian" and the axis of fifth metatarsal bone. Point L is artificially determined at the midpoint of the outer lateral of the arch. Thus, please note the 50 % in Fig. 8 has a different benchmark.

Participant is asked to provide a series of clinical information of gender, age, height, weight, foot length, foot width, foot health, shoe-wearing habits, daily average steps, and exercise habits before each test. During the test, the volunteer sequentially places five test positions on the detectors of three stress-strain detecting units (tensile/compression, shear in two directions, and torsion) for the corresponding test. To ensure the data accuracy, each test is repeated three times, that is, 60 tests in total for one subject.

In this work, the amplitude of reciprocal and shearing test is set to be ± 2 mm, the twist range of torsion test is set to be $\pm 14^{\circ}$. The amplitude is chosen by observing the regular motion of healthy plantar pad, and the frequency is determined by an empirical upper limit of human foot usage in common sense, and higher frequency may cause noticeably discomfort on subject [40]. It is important to note that the displacement in real test is not exact the setup value (± 2 mm or $\pm 14^{\circ}$), due to the test conditions and characteristics of subject, the difference could be unignorable, therefore the strain must also be preciously measured to calculate the moduli. The reciprocal motion is processed for 10 s. In practice, the oscillation begins at a lower frequency and reaches its set frequency after 1 s. Typically, it takes around 2 s for the signal to become stable, so we take the data after $t = 4$ s to calculate the average force and errors.

5.2. *Test protocol for mimic foot model and brick sample*

Furthermore, as silica rubber of particular grade is utilized to prepare the "standard sample" in this research, we have prepared a SR foot model with the same grade for test, as a reference comparison to the living plantar. The model is extracted and rebuilt from CT

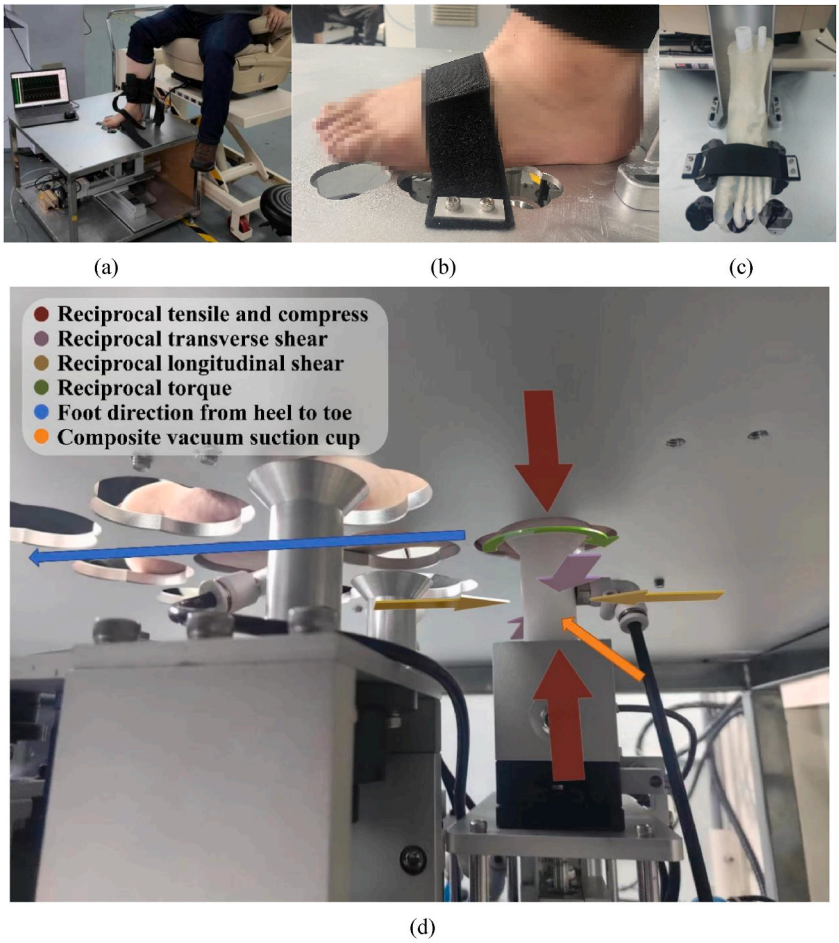

Fig. 9. The test device and setup: (a) the general test posture; (b) the test setup of volunteer's foot (the resolution of foot is downgraded for privacy protection); (c) the test setup of SR foot model; (d) the test setup from undercover view. (The figure has been publicly disclosed, and copyrights for re-use are authorized in this paper.)

scan of real foot. Sectional foot images were obtained through CT imaging of the right foot of a volunteer subject, who was fully informed and signed the consent form before trials. Image of a specific density range (i.e., soft tissue or bone) was distinguished using MIMICS software (Materialise, Leuven/Belgium). The surface reverse modeling of soft tissue and bone was completed by the 3D reconstruction tool Geomagic Studio (3D Systems, Morrisvillerth Carolina). The bone was 3D-printed with PLA resin. The mold is obtained through Boolean operation on soft tissue and a cubic model. Subsequently, the 3D-printed bone is fixed inside the mold, followed by the casting of silicone gel to make mimic foot. Fig. 9 shows the general test posture (Fig. 9a), the subject foot and mimic foot model positioning (Fig. 9b and c), and a direct view of detection (Fig. 9d). The test conditions on mimic foot model and brick sample are similar to the volunteer participant. The videos of tests on living foot and SR mimic foot are attached in supplementary materials as a visual presentation of the test.

6. Preliminary results and discussion

The living test results on the volunteer's plantar soft tissue are presented in Fig. 10. There are 4 subfigures classified by four types of stress-strain behaviors (tensile/compression (Fig. 10 a), longitudinal shear (Fig. 10 b), transverse shear (Fig. 10 c), and torsion (Fig. 10 d)) on five spots (M1, M2, M5, L and H). In all the four types of tests, we intendedly reverse the directions of displacement and force to present a peak-to-valley view for a clear observation. In the results of tensile/compression, the peak in the force curve represents the compression (push up) with a valley on the displacement, and vice versa. In shear and torsion, the stress is symmetrical thus the direction is trivial. For a better demonstration, the sixty periods of signals of three trials (twenty periods in one trial) are overlapped to be cloud curves and the average of each are presented as solid line in Fig. 10.

It can be observed that the periodic signals behave stable in amplitude and extremum, which confirms the preciousness of the device and method. Since the stability of test quite depends on the cooperation of the subject, the results are much more stable within in one trial, whereas the signal overlap of different trials may sometime generate noticeable noise, e.g., the tensile/compression force of the fifth metatarsal head in Fig. 10 a, though the deviations are still in acceptable range.

The same tests have also been done on the five spots of the SR mimic foot model and brick sample described in section 4. The measured force, strain and calculated moduli are summarized in Table 2. All data are presented as mean values ± standard deviations, and they are found to be generally consistent and reasonable. These calculated T/C and shear moduli values fall within those obtained from others' previous experimental measurements on plantar soft tissue, ranging from 0.05 to 0.3 MPa under strains of 10–35 % [41–43]. The displacements (strain) in each test mode are stable respectively with acceptable deviations. It is observed that the stress and strain are mutually correlated, for example the five T/C tests on living plantar roughly presents negative relation between force and strain, i.e., higher force is paired with smaller strain. This agrees with our common sense that if a subject is "hard" to deform, it

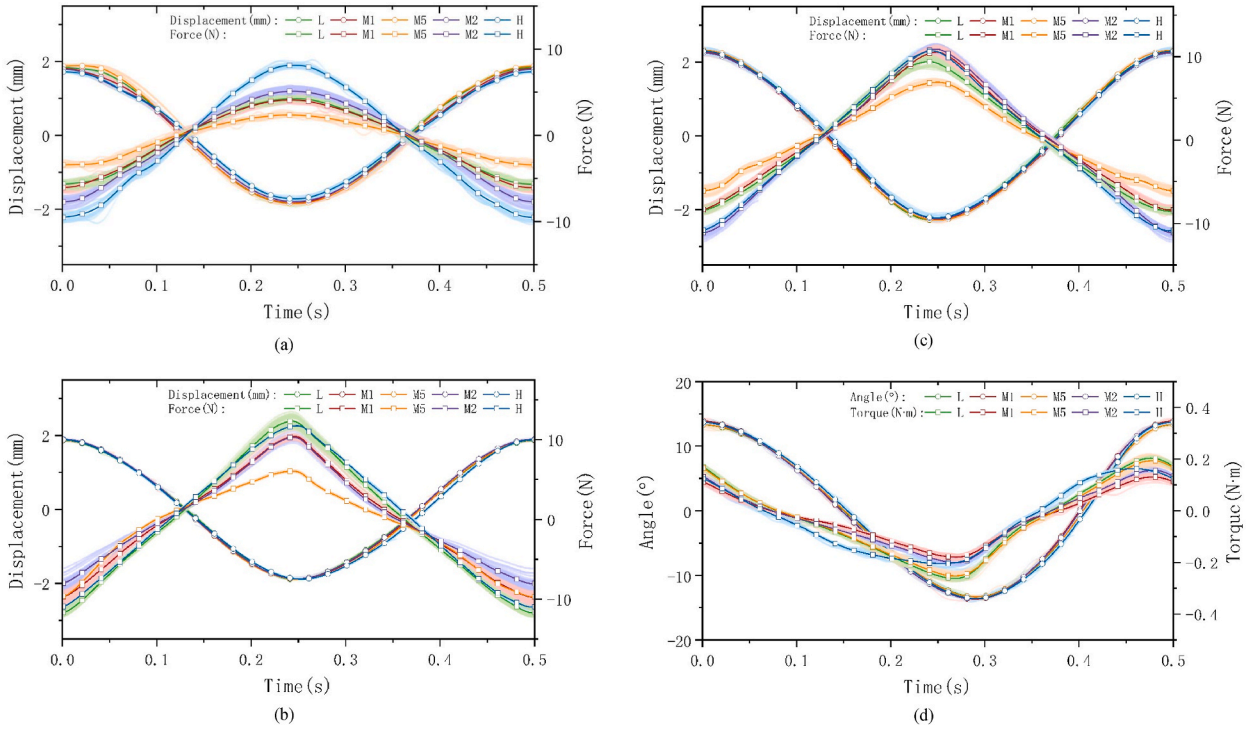

Fig. 10. The stress-strain behaviors of four types: tensile/compression, longitudinal shear, transverse shear, and torsion of a volunteer's plantar soft tissue at the various spots: the first, second, and fifth metatarsal heads (M1, M2, and M5), midpoint of lateral edge (L), and Heel (H): (a) the tensile/compression; (b) longitudinal shear; (c) transverse shear; (d) torsion on the five test spots respectively.

Table 2
The results of tests on living heel and inorganic samples.

	Tensile/ Compress Force (N)	Displacement (mm)	Analog T/C Modulus H_{TC} (MPa)	Longitudinal Shear Force *(N)*	Displacement (mm)	Analog Shear Modulus H_{LS} (MPa)	Transverse Shear Force *(N)*	Displacement (mm)	Analog Shear Modulus H_{TS} (MPa)	Torque *(N·m)*	Displacement (Degree)	Analog Torsion Modulus *HT* (N·mm^2)
H	17.6948 ± 0.8400	3.5049 ± 0.0745	0.1469	22.7176 ± 0.0243	3.7892 ± 0.0034	0.1578	21.6163 ± 0.0774	4.5529 ± 0.0043	0.1249	0.3725 ± 0.0158	27.3575 ± 0.0199	7884.8191
L	9.9714 ± 0.5182	3.6945 ± 0.0136	0.086	24.0589 ± 0.8181	3.7837 ± 0.0038	0.1673	17.9712 ± 0.6877	4.5953 ± 0.004	0.1029	0.4636 ± 0.0077	26.7939 ± 0.0563	10146.1483
M1	10.2026 ± 0.3446	3.6472 ± 0.0062	0.0891	20.1302 ± 0.6391	3.7838 ± 0.003	0.1400	19.0177 ± 0.5991	4.5604 ± 0.0114	0.1097	0.2977 ± 0.0043	27.8841 ± 0.0151	6185.7673
M2	12.8567 ± 0.356	3.5947 ± 0.0023	0.1139	18.3147 ± 0.4653	3.7931 ± 0.0051	0.1271	22.1472 ± 0.0177	4.5339 ± 0.0022	0.1285	0.3633 ± 0.0137	27.4106 ± 0.0876	7589.7347
M5	5.8686 ± 0.1831	3.734 ± 0.0177	0.0501	15.6053 ± 0.2343	3.7865 ± 0.0019	0.1085	13.0486 ± 0.4957	4.6438 ± 0.0196	0.0739	0.4317 ± 0.0081	26.9244 ± 0.002	9366.9184
mimic foot H	31.5732 ± 0.2521	2.8429 ± 0.0226	0.3537	33.4994 ± 0.8667	3.5002 ± 0.0053	0.2519	17.1526 ± 1.1266	3.5767 ± 0.0138	0.1262	0.6802 ± 0.0388	22.0088 ± 0.299	17770.4704
mimic foot *L*	26.1194 ± 0.0226	2.8663 ± 0.0316	0.2902	40.771 ± 3.5223	3.478 ± 0.0114	0.3085	37.2013 ± 1.3878	3.3908 ± 0.01	0.2887	0.6603 ± 0.0292	21.9049 ± 0.2269	17262.8910
mimic foot M1	32.268 ± 0.012	2.825 ± 0.02	0.3638	42.9486 ± 1.99	3.4608 ± 0.0046	0.3266	35.0771 ± 1.544	3.4346 ± 0.0335	0.2688	0.9181 ± 0.0308	20.1083 ± 0.1761	26151.1449
mimic foot M2	29.6729 ± 0.0316	2.8399 ± 0.0206	0.3328	37.7017 ± 1.7231	3.476 ± 0.0088	0.2854	37.0456 ± 1.1805	3.428 ± 0.0186	0.2844	1.296 ± 0.0341	16.7639 ± 0.3431	44295.5314
mimic foot M5	30.5515 ± 0.0497	2.834 ± 0.0116	0.3433	39.2377 ± 1.065	3.4703 ± 0.0042	0.2975	34.611 ± 0.7972	3.4441 ± 0.0066	0.2645	0.7779 ± 0.0816	20.9156 ± 0.61	21303.7420
SR brick sample[a]	23.0096 ± 1.3153	3.0253 ± 0.0076	0.2422	40.3724 ± 1.2456	3.6145 ± 0.0026	0.2939	/	/	/	1.3636 ± 0.0258	21.1032 ± 0.0305	37023.3077

[a] The brick sample is homogeneous in horizontal thus the shear direction is regardless.

costs larger force and less deformation. Given that the H_{TC} of various spots are significantly different, the small deviations on strains confirms the preciousness of the machine and test method. Furthermore, we compared the distribution of T/C and shear moduli along various spots between volunteer and mimic foot, as shown in Fig. 11. The H_{TC} of mimic foot model are relatively more consistent, that is also expectable since the mimic model is more homogenous with uniform material and texture. And the higher moduli of mimic model imply the grade of SR employed here maybe slightly "stiffer" to mimic the plantar tissue, at least for this individual case. Furthermore, the SR brick sample presents even larger force, smaller strain and higher modulus in every category, which reflects the effects of size and shape, and it again imprints the necessity of sample standardization and calibration discussed in section 4.

Another interesting finding in Fig. 11 is that the transverse shear modulus of the heel of mimic foot presents significant derivation from other points. This deviation is not observed in the volunteer test. This result is an average of multiple repeated experiments, which reduces the likelihood of operational error. It may imply that the geometric feature of heel is quite unique, and significant anatomical structure and material properties of heel tissue make it real modulus normal to other parts of plantar. Although further research with more reality tests and analysis are necessary to validate and comprehend this hypothesis, this observation provides support for the plausibility of the definition of "apparent modulus."

Moreover, several interesting observations on the data can induce some intuitive conclusions. For the T/C test, the M2 and H spot have the higher modulus, whereas these two are considered to be most load-bearing spots on the plantar, therefore the fact that they have better material property accords well to a previous report on the compressive material properties of the cadaveric plantar specimens [20]. And the H spot is even higher than M2 while the heel has less bearing area than forefoot. The T/C modulus of the M2 is higher than the M1. This is because the center of normal stress (pressure) is applied to the 2nd metatarsal head during walking [44,45], and leads to an increase in modulus. In the two modes of shearing test, only spot L presents large difference in longitudinal and transverse. This discrepancy can be attributed to the heterogeneity in its geometry, which can be readily hypothesized. The H_{LS} is much larger, whereas the foot arch mainly bears shearing along longitudinal direction during daily walking, and shearing in the other direction is rare. In comparison to forefoot regions, the heel exhibits relatively high compressive and shear moduli and skin thickness, which is consistent with the reported result on the compressive and shear characteristics of diabetic plantar tissue [46]. Biomechanically, ground contact begins at the heel during walking, hence a thicker, stiffer, more elastic layer of soft tissue at this point may

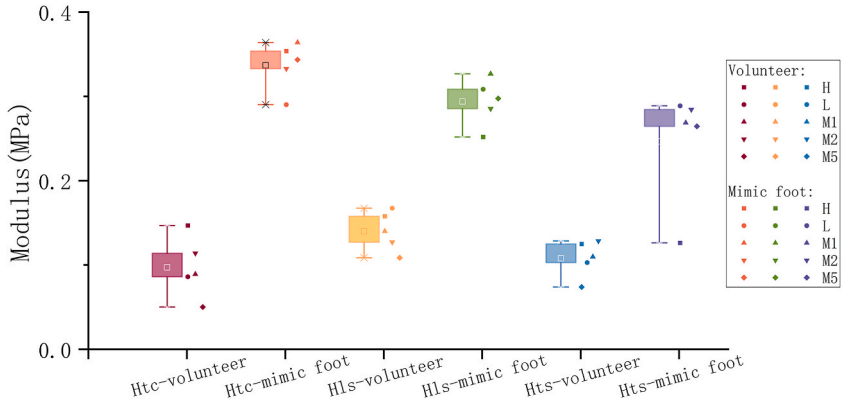

Fig. 11. The distribution of tensile/compression and shear moduli along various spots between volunteer and mimic foot: The box is percentage of 25–75, the bar is the maximum and minimum value, the detailed distributions of data point are presented aside.

help in load absorption, explaining that plantar ulcers often occur in the forefoot rather than the heel [47,48]. Another impressive observation is that the H_T of M5 is much larger than other spots. Torsion is a rarely mentioned stress in the study of foot and plantar mechanics, and there has been no published report on this topic to the best of authors' knowledge. However, it is also a common daily experience, that when we turn around during walking, it usually starts exerting force from the outer part of the forefoot, that is the M5.

Additionally, it is well recognized that viscoelasticity is the primary measure used to describe the mechanical properties of soft tissues [49–52]. Nevertheless, the current test conditions did not reveal any viscoelasticity in tensile/compression and shear, as seen by the absence of phase lag in Fig. 10a, b, and c. However, Fig. 10d clearly demonstrates a noticeable phase lag in torsion. Given the fact that different elastomeric materials have varying frequency ranges in which they exhibit viscoelastic behavior, additional research is necessary to identify and comprehend the viscosity of the plantar tissue.

Though these intuitive observations are still far away from scientific hypothesis and facts, which relies on the establishment of a big dataset to make sound conclusions, and these results measured could also possibly be due to the individual features, rather than common properties of human plantar, further investigations based on a large number of participants tested are necessary to find general laws. Better still, the agreements of above findings to our common sense are good encouragements on this novel in-situ DMA method. Since this manuscript is mainly to demonstrate our newly-invented device and establish the methodology, we are not going to further analyze the data and their correlations to the foot health. Future work in depth will be reported based on a decent number of tests with a collection of sufficient data, and is in progress in our group.

7. Conclusion and perspective

This study is expected to establish a novel method, which is inspired by the DMA in classical material science to obtain periodical strain-stress behavior to analyze the viscoelasticity of elastomer, especially the plantar soft tissue. The main novelty is to overcome the difficulty of in-situ characterization on the mechanical properties of biological soft tissues via fixing soft tissues by vacuum suction cups, and obtain *in-vivo* mechanical properties of living plantar. Three types of mechanism: tensile/compression, shear, and torsion are designed and four modes of tests are applied on five particular chosen spots on the living plantar. The results show good preciousness and consistence, and several interesting intuitive correlations are observed in the volunteer and mimic sample tests data, which well encourages the subsequent systematic researches in the future. This in-situ DMA methodology is expected to have potential applications in biomechanical theory, clinical diagnosis and footcare engineering application.

Additionally, this new technique is also expected to make substantial contributions to the finite element analysis (FEA), which is a common tool in biomechanical analysis, but always being accused by the lack of the material parameters in reality, by providing the direct realistic material properties, and a decent standard to check the simulation. Hopefully more complex anisotropy finite element models of foot can be built with the foundation of the data measured by the device.

Nonetheless, it is still clear that there are limitations to the existing research and challenges ahead. As stated, a set of "moduli" similar to the classical modulus are defined with measurable strain and stress. With incorporating the characteristic length as an internal part of the "apparent property" of subject, we found it is practical to setup a nominal original length, as 10 mm in this work, to make parallel comparison among the test results. However, the possibility and necessity to determine an effective "equivalent length" L to characterize the "eigen property" of subject, especially for those of complex shape and size, remained to be a challenge.

Furthermore, it is an intrigued question that if there exists firm relationship between the newly defined modulus and the classical modulus. These uncertainties are expected to be answered in the future research on a large number of tests and collection of data on various living subjects and inorganic samples, with the help of machine learning. The establishment of big dataset on the plantar can also enhance the development of our in-situ DMA method and perhaps expand its application to other types of soft tissue, particularly those with extremely low stiffness, such as the brain, which are vulnerable and challenging to be tested [53–55].

Finally, the most captivating aspect of this study centers around the clinics. The diagnostic and health monitoring value of foot

illness and footcare can only be accurately determined through the analysis of a comprehensive dataset, as these indicators are relatively new in the field of biology and health. Although the current work only reported a single subject for exemplary demonstration. In the near future, we intend to conduct a comprehensive and precise series of clinical tests on a broad scale. These tests will involve gathering incremental personal and clinical data, which will be analysed to identify more critical correlations.

Ethics statement

The Ethical Review Committee of Huashan Hospital, Fudan University (HIRB) approves the ethical review, with Ethics Approval No.: (2022) Temporary Trial No. (889). The authors confirm that the study complies with all regulations, and informed consent was obtained from the participants.

Data availability statement

The full data generated or analysed to support the conclusion during this study are included in this published article and its supplementary information files.

CRediT authorship contribution statement

Longyan Wu: Writing – original draft, Software, Investigation, Data curation. **Ran Huang:** Writing – review & editing, Writing – original draft, Validation, Supervision, Resources, Project administration, Methodology, Investigation, Funding acquisition, Formal analysis, Data curation, Conceptualization. **Lisheng Tang:** Validation, Investigation. **Xinyi Ning:** Formal analysis, Data curation. **Jun Zhu:** Validation, Supervision, Resources. **Xin Ma:** Supervision, Project administration, Funding acquisition.

Declaration of competing interest

The authors declare that they have no known competing financial interests or personal relationships that could have appeared to influence the work reported in this paper.

Acknowledgement

This work is financially supported by the National Key Research and Development Program China (2022YFC2009500), the Medical Engineering Fund of Fudan University (YG2021-005, YG2022-008), the Fudan-Yiwu Fund (FYX-23-102), and the TZI-ZJU Industrial Program (2022ZSS09, 2023CLG01, 2023CLG01PT). The authors sincerely appreciate Ms. Ren Huang for graphical artwork.

Appendix A. Supplementary data

Supplementary data to this article can be found online at https://doi.org/10.1016/j.heliyon.2024.e29986.

References

[1] A.N. Natali, C.G. Fontanella, E.L. Carniel, Constitutive formulation and analysis of heel pad tissues mechanics, Med. Eng. Phys. 32 (5) (2010) 516–522.
[2] R.L.C. Kwan, Y.P. Zheng, G.L.Y. Cheing, The effect of aging on the biomechanical properties of plantar soft tissues, Clin. BioMech. 25 (6) (2010) 601–605.
[3] H. Özdemır, Y. Söyüncü, M. Özgörgen, et al., Effects of changes in heel fat pad thickness and elasticity on heel pain, J. Am. Podiatr. Med. Assoc. 94 (1) (2004) 47–52.
[4] A.N. Natali, C.G. Fontanella, E.L. Carniel, A numerical model for investigating the mechanics of calcaneal fat pad region, J. Mech. Behav. Biomed. Mater. 5 (1) (2012) 216–223.
[5] H. Ye, K. Zhang, D. Kai, et al., Polyester elastomers for soft tissue engineering, Chem. Soc. Rev. 47 (12) (2018) 4545–4580.
[6] A. Cichowitz, W.R. Pan, M. Ashton, The heel: anatomy, blood supply, and the pathophysiology of pressure ulcers, Ann. Plast. Surg. 62 (4) (2009) 423–429.
[7] Y.N. Wang, K. Lee, J.B. Shofer, W.R. Ledoux, Histomorphological and biochemical properties of plantar soft tissue in diabetes, Foot 33 (2017) 1–6.
[8] W. Kang, Y. Zhang, W. Bu, et al., Statistical analysis of mechanical properties of biological soft tissue under quasi-static mechanical loading, Med. Novel Technol. Devices 17 (2023) 100202.
[9] W.R. Ledoux, D.F. Meaney, H.J. Hillstrom, A quasi-linear, viscoelastic, structural model of the plantar soft tissue with frequency-sensitive damping properties, J. Biomech. Eng. 126 (6) (2004) 831–837.
[10] U.C. Ugbolue, E.L. Yates, K.E. Rowland, S.C. Wearing, Y. Gu, W.K. Lam, J.S. Baker, N.F. Sculthorpe, F. Dutheil, A novel simplified biomechanical assessment of the heel pad during foot plantarflexion, Proc. IME H J. Eng. Med. 235 (2) (2021) 197–207.
[11] S.C. Wearing, S.L. Hooper, P. Dubois, J.E. Smeathers, A. Dietze, Force-deformation properties of the human heel pad during barefoot walking, Med. Sci. Sports Exerc. 46 (8) (2014) 1588–1594.
[12] V. Campanelli, M. Fantini, N. Faccioli, A. Cangemi, A. Pozzo, A. Sbarbati, Three-dimensional morphology of heel fat pad: an *in vivo* computed tomography study, J. Anat. 219 (5) (2011) 622–631.
[13] K.P. Menard, N. Menard, Dynamic Mechanical Analysis, CRC press, 2020.
[14] M. Ginic-Markovic, N.R. Choudhury, M. Dimopoulos, D.R.G. Williams, J. Matisons, Characterization of elastomer compounds by thermal analysis, Thermochim. Acta 316 (1) (1998) 87–95.
[15] G. Grigoriadis, N. Newell, D. Carpanen, A. Christou, A.M. Bull, S.D. Masouros, Material properties of the heel fat pad across strain rates, J. Mech. Behav. Biomed. Mater. 65 (2017) 398–407.

[16] T. Negishi, K. Ito, A. Kamono, T. Lee, N. Ogihara, Strain-rate dependence of viscous properties of the plantar soft tissue identified by a spherical indentation test, J. Mech. Behav. Biomed. Mater. 102 (2020) 103470.
[17] A. Gefen, Plantar soft tissue loading under the medial metatarsals in the standing diabetic foot, Med. Eng. Phys. 25 (6) (2003) 491–499.
[18] C.C. Hsu, W.C. Tsai, C.P.C. Chen, et al., Effects of aging on the plantar soft tissue properties under the metatarsal heads at different impact velocities, Ultrasound Med. Biol. 31 (10) (2005) 1423–1429.
[19] T.C. Hsu, C.L. Wang, W.C. Tsai, et al., Comparison of the mechanical properties of the heel pad between young and elderly adults, Arch. Phys. Med. Rehabil. 79 (9) (1998) 1101–1104.
[20] W.R. Ledoux, J.J. Blevins, The compressive material properties of the plantar soft tissue, J. Biomech. 40 (13) (2007) 2975–2981.
[21] S. Pai, W.R. Ledoux, The compressive mechanical properties of diabetic and non-diabetic plantar soft tissue, J. Biomech. 43 (9) (2010) 1754–1760.
[22] J. Lekkala, Plantar shear stress measurements-A review, Clin. BioMech. 29 (5) (2014) 475–483.
[23] T. Stief, K. Peikenkamp, A new insole measurement system to detect bending and torsional moments at the human foot during footwear condition: a technical report, J. Foot Ankle Res. 8 (1) (2015) 1–8.
[24] W.C. Wang, W.R. Ledoux, B.J. Sangeorzan, et al., A shear and plantar pressure sensor based on fiber-optic bend loss, J. Rehabil. Res. Dev. 42 (3) (2005) 315–326.
[25] L. Wu, J. Zhu, J. Zheng, X. Geng, X. He, L. Tang, R. Huang, X. Ma, A novel dynamic mechanical analysis device to measure the *in-vivo* material properties of plantar soft tissue and primary finite elementary analysis results, J. Phys. Conf. 2313 (2022) 012029.
[26] R. Huang, J. Zhu, L. Wu, X. Ma, In Vivo Multidimensional Stress-Strain Testing Device for Plantar Soft Tissues (China Patent No. 202211260514.1; PCT Application No. PCT/CN2023/095205), China National Intellectual Property Administration, 2023.
[27] L. Wu, L. Tang, R. Huang, Determination of the ignorable boundary condition and standard sample for A novel in-situ dynamic mechanical analysis method on soft matter, J. Phys. Conf. 2612 (2023) 012014.
[28] J.T.M. Cheung, M. Zhang, A 3-dimensional finite element model of the human foot and ankle for insole design, Arch. Phys. Med. Rehabil. 86 (2) (2005) 353–358.
[29] J.E. Miller-Young, N.A. Duncan, G. Baroud, Material properties of the human calcaneal fat pad in compression: experiment and theory, J. Biomech. 35 (12) (2002) 1523–1531.
[30] L. Zhao, Y. Zhang, Z. Yin, Training path optimization method of a moveable multifunction rehabilitation robot, IEEE Rob. Autom. Lett. 8 (3) (2023) 1651–1658.
[31] I.M. Hasan, E.Q. Yumbla, W. Zhang, Development of a Soft Inflatable Exosuit for Knee Flexion Assistance//2022 9th IEEE RAS/EMBS International Conference for Biomedical Robotics and Biomechatronics (BioRob), IEEE, 2022, pp. 1–6.
[32] X. Zhang, H. Yi, J. Liu, et al., A bio-inspired compliance planning and implementation method for hydraulically actuated quadruped robots with consideration of ground stiffness, Sensors 21 (8) (2021) 2838.
[33] Z. Li, C. Liu, Y. Han, et al., Design, fabrication and experiments of a hydraulic active-passive hybrid prosthesis knee, Technol. Health Care 31 (4) (2023) 1267–1277.
[34] O. Postolache, A.L. Ribeiro, H.G. Ramos, GMR array uniform eddy current probe for defect detection in conductive specimens, Measurement 46 (10) (2013) 4369–4378.
[35] C. Price, C. Nester, Foot dimensions and morphology in healthy weight, overweight and obese males, Clin. BioMech. 37 (2016) 125–130.
[36] S. Forghany, D.R. Bonanno, H.B. Menz, et al., An anatomically-based masking protocol for the assessment of in-shoe plantar pressure measurement of the forefoot, J. Foot Ankle Res. 11 (2018) 1–9.
[37] A.K. Ramanathan, P. Kiran, G.P. Arnold, et al., Repeatability of the Pedar-X® in-shoe pressure measuring system, Foot Ankle Surg. 16 (2) (2010) 70–73.
[38] T.C. Pataky, Spatial resolution in plantar pressure measurement revisited, J. Biomech. 45 (12) (2012) 2116–2124.
[39] J. Tang, D.L. Bader, D. Moser, et al., A wearable insole system to measure plantar pressure and shear for people with diabetes, Sensors 23 (6) (2023) 3126.
[40] Usain Bolt's world record for the 100-meter sprint is 9.58 seconds, taking approximately 41 steps, that is about four steps per second, i.e., two single plantar landings. Therefore, 2Hz Can Be Considered the Upper Limit of Human Foot Usage under Full Load Conditions.
[41] J.T.M. Cheung, M. Zhang, A.K.L. Leung, et al., Three-dimensional finite element analysis of the foot during standing—a material sensitivity study, J. Biomech. 38 (5) (2005) 1045–1054.
[42] A. Gefen, M. Megido-Ravid, Y. Itzchak, *In vivo* biomechanical behavior of the human heel pad during the stance phase of gait, J. Biomech. 34 (12) (2001) 1661–1665.
[43] Y.P. Zheng, Y.K.C. Choi, K. Wong, et al., Biomechanical assessment of plantar foot tissue in diabetic patients using an ultrasound indentation system, Ultrasound Med. Biol. 26 (3) (2000) 451–456.
[44] M. Ko, L. Hughes, H. Lewis, Walking speed and peak plantar pressure distribution during barefoot walking in persons with diabetes, Physiother. Res. Int. 17 (1) (2012) 29–35.
[45] A. Amemiya, H. Noguchi, M. Oe, et al., Shear stress-normal stress (pressure) ratio decides forming callus in patients with diabetic neuropathy, J. Diabetes Res. 2016 (2016) 3157123.
[46] L. Brady, S. Pai, J.M. Iaquinto, et al., The compressive, shear, biochemical, and histological characteristics of diabetic and non-diabetic plantar skin are minimally different, J. Biomech. 129 (2021) 110797.
[47] A.J.M. Boulton, The diabetic foot, Medicine 47 (2) (2019) 100–105.
[48] A. Caselli, H. Pham, J.M. Giurini, et al., The forefoot-to-rearfoot plantar pressure ratio is increased in severe diabetic neuropathy and can predict foot ulceration, Diabetes Care 25 (6) (2002) 1066–1071.
[49] X. Ning, Q. Zhu, Y. Lanir, S.S. Margulies, A transversely isotropic viscoelastic constitutive equation for brainstem undergoing finite deformation, J. Biomech. Eng. 128 (6) (2006) 925–933.
[50] W. Li, D.E.T. Shepherd, D.M. Espino, Dynamic mechanical characterization and viscoelastic modeling of bovine brain tissue, J. Mech. Behav. Biomed. Mater. 114 (2021) 104204.
[51] W. Li, D.E.T. Shepherd, D.M. Espino, Investigation of the compressive viscoelastic properties of brain tissue under time and frequency dependent loading conditions, Ann. Biomed. Eng. 49 (2021) 3737–3747.
[52] W. Kang, L. Wang, Y. Fan, Viscoelastic response of gray matter and white matter brain tissues under creep and relaxation, J. Biomech. 162 (2024) 111888.
[53] A.F. Christ, K. Franze, H. Gautier, P. Moshayedi, J. Fawcett, R.J. Franklin, R.T. Karadottir, J. Guck, Mechanical difference between white and gray matter in the rat cerebellum measured by scanning force microscopy, J. Biomech. 43 (15) (2010) 2986–2992.
[54] K. Laksari, M. Shafieian, K. Darvish, Constitutive model for brain tissue under finite compression, J. Biomech. 45 (4) (2012) 642–646.
[55] W. Kang, P. Xu, Y. Yue, L. Wang, Y. Fan, Difference analysis of phenomenological models with two variable forms for soft tissue quasi-static mechanical characterization, Comput. Biol. Med. 150 (2022) 106150.